JOURNAL OF AIRCRAFT
Vol. 32, No. 5, September–October 1995

De-Dopplerization of Aircraft Acoustic Signals

Jeffrey J. Kelly* and Mark R. Wilson†
Lockheed Engineering and Sciences Company, Inc., Hampton, Virginia 23666-1339

A de-Dopplerization scheme is devised and applied to both a tonal noise source, an XV-15 aircraft, and a broadband noise source, an F-18 aircraft. The procedure is developed from the conservation equations of fluid mechanics and is described in the article. The de-Dopplerized time history is constructed by using linear interpolation in the measured time history. This was made possible by knowing the position history of the aircraft provided by radar and/or laser tracking. The XV-15 data established that the scheme can accurately account for Doppler frequency shifts. The F-18 data confirms what has been noted in prediction models and static tests pertaining to broadband shock-associated noise. That is, the peak frequency increases and the peaks broaden toward the jet axis. Another issue addressed in the study is the influence of correcting for spherical spreading and Doppler amplitude on the spectral shape and overall sound pressure levels of the source. Results from this investigation confirm that the dominant noise source in high-speed jets is due to turbulent mixing.

Nomenclature

c_0 = ambient speed of sound
f = frequency
f_R = Doppler shifted frequency
f_S = source frequency
$\boldsymbol{f}$ = momentum source vector
h = aircraft altitude
L = sound-pressure level at the observer
L_m = sound-pressure level at the source
$\boldsymbol{M}$ = convection Mach number vector
$\boldsymbol{M}_A$ = aircraft Mach number vector
$\boldsymbol{n}_r$ = unit vector in the direction of $\boldsymbol{r}(\tau)$
P_m = Fourier transform of source pressure
P_1 = Fourier transform of measured pressure
p = pressure
p_1 = acoustic pressure
q = mass source function
$\boldsymbol{r}$ = position vector between source and receiver at time τ
r_m = reference distance
T_t = window duration of measured signal
T_τ = window duration of source signal
t = reception time
$\boldsymbol{U}$ = aircraft velocity vector
$\boldsymbol{x}$ = position vector
$\boldsymbol{x}_s$ = source position vector
$\Delta\theta$ = smear angle
θ, ϕ = source directivity angles
θ_1 = directivity angle at time τ_1
τ = emission time

Introduction

IT is well known that motion of a sound source will produce an altered acoustic field compared to the static field. The change in acoustic parameters resulting from the kinematics of the source are usually characterized as due to source modification and forward flight or convection effects. This study concerns the latter topic (forward flight). The most obvious feature of source motion is frequency (Doppler) shifts. To a static observer, this is often explained by shifts in discrete tones in spectra. But, in reality, the signal is nonstationary to a fixed observer and signal processing procedures will produce smeared or broadened spectra. De-Dopplerization schemes for acoustic signals have been previously addressed.[1,2] Less obvious is the change in pressure amplitude caused by motion. This has now become an issue because of its possible impact on community noise standards by future aircraft, especially the High-Speed Civil Transport (HSCT). Also, since the amplitude varies in time, it contributes to the nonstationarity of the signal. Thus, correcting for Doppler amplitude changes could enhance any de-Dopplerization schemes.[3]

De-Dopplerized versions of the measured ground data for a particular aircraft can provide a reasonably stationary signal characterizing the noise sources of the aircraft. The reconstructed signal alleviates spectral smearing and allows comparison of spectral features with physical mechanisms of the source. Since aircraft noise is usually quantified by static tests for both full-scale and model wind-tunnel measurements, de-Dopplerization of flight test data facilitates its comparison to static data. This study considers correcting for spherical spreading and Doppler amplitude along with frequency in the time history of the recorded signal in order to render it approximately stationary. These corrections also aid in determining noise source directivity. The de-Dopplerization technique is applied to both a tonal source and a broadband source. Data acquired during a XV-15 tilt-rotor test is the tonal example and that acquired from F-18 jet aircraft flyovers is the broadband example.

Governing Equations Describing Source Motion

A common model for analyzing acoustic source motion is to include source terms in the mass and momentum equations. Assuming small acoustic disturbances, the governing equations can be linearized. The linear equations can be combined to yield the following nonhomogeneous wave equation for the acoustic pressure in a stationary (i.e., ground-based) reference frame

$$c_0^{-2}\frac{\partial^2 p_1}{\partial t^2} - \nabla^2 p_1 = \frac{\partial q}{\partial t} - \nabla\cdot\boldsymbol{f} \tag{1}$$

Equation (1) has a solution that can be stated in terms of volume integrals.[4] Considering the source structure to be composed of a superposition of moving point sources allows the volume integrals to be evaluated in a closed form.[5]

Presented as Paper 93-0737 at the AIAA 31st Aerospace Sciences Meeting and Exhibit, Reno, NV, Jan. 11–14, 1993; received April 21, 1993; revision received Feb. 24, 1995; accepted for publication Feb. 28, 1995.

*Staff Engineer, 144 Research Drive. Senior Member AIAA.
†Senior Associate Engineer, 144 Research Drive. Member AIAA.

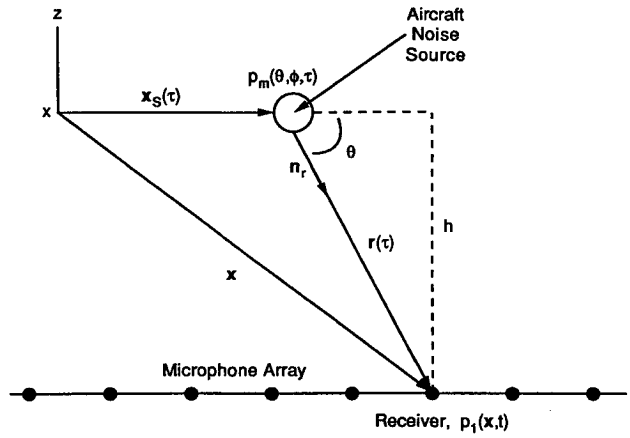

Fig. 1 Level flyover geometry.

In the far field, r^{-1} terms dominate and for uniform motion, acceleration terms vanish. Also, in the far field, the position vectors $\boldsymbol{r}$ of each source are approximately equal. Making the assumption that each source moves at the same velocity and implementing the above observations allows the total radiated pressure to be written as

$$p_1(\boldsymbol{x}, t) = \frac{p_m(\theta, \phi, \tau)}{[r(\tau)/r_m][1 - \boldsymbol{M}(\tau)\cdot\boldsymbol{n}_r(\tau)]^2} \tag{2}$$

Here, $p_m(\theta, \phi, \tau)$ has been introduced to describe the source structure in terms of pressure at the reference distance r_m. A geometrical description of this situation is shown in Fig. 1, and $\boldsymbol{r}$ is given by

$$\boldsymbol{r}(\tau) = \boldsymbol{x} - \boldsymbol{x}_s(\tau) \tag{3}$$

where $\boldsymbol{x}_s$ represents the position history of the aircraft. It is important to distinguish between reception time t and emission or retarded time τ in Eq. (2), which are related by

$$t = \tau + [r(\tau)/c_0] \tag{4}$$

In the above expression, τ is the time of signal emission and t is the time of signal reception.

Spectral Relations and Sound Pressure Level

The relation between the ground spectrum determined from $p_1(\boldsymbol{x}, t)$ and the source spectrum determined from $p_m(\theta, \phi, \tau)$ is now considered. Equation (2) is altered to have an arbitrary value of the exponent on the Doppler amplitude factor:

$$p_1(\boldsymbol{x}, t) = \frac{p_m(\theta, \phi, \tau)}{[r(\tau)/r_m][1 - \boldsymbol{M}(\tau)\cdot\boldsymbol{n}_r(\tau)]^n} \tag{5}$$

This change to arbitrary n instead of the theoretically derived value of $n = 2$ is done because of questions raised[6] about the high-pressure levels that Eq. (5) predicts as M approaches 1.0 if n is equal to 2. Performing the finite Fourier transform of Eq. (5) in t results in

$$P_1(\boldsymbol{x}, f) = \int_{t_1}^{t_2} p_1(\boldsymbol{x}, t)e^{-j2\pi ft}\,dt = r_m \int_{t_1}^{t_2} \frac{p_m(\theta, \phi, \tau)e^{-j2\pi ft}\,dt}{r(\tau)[1 - \boldsymbol{M}(\tau)\cdot\boldsymbol{n}_r(\tau)]^n} \tag{6}$$

This can be expressed in terms of τ by way of Eq. (4), which permits the following substitution:

$$dt = [1 - \boldsymbol{M}(\tau)\cdot\boldsymbol{n}_r(\tau)]\,d\tau \tag{7}$$

Thus, in terms of emission time, Eq. (6) becomes

$$P_1(\boldsymbol{x}, f) = r_m \int_{\tau_1}^{\tau_2} \frac{p_m(\theta, \phi, \tau)\exp\{-j2\pi f[\tau + r(\tau)/c_0]\}\,d\tau}{r(\tau)[1 - \boldsymbol{M}(\tau)\cdot\boldsymbol{n}_r(\tau)]^{n-1}} \tag{8}$$

The window durations of the measured signal and the source signal are, respectively, defined as

$$T_t = t_2 - t_1 \tag{9}$$

$$T_\tau = \tau_2 - \tau_1 \tag{10}$$

It is easily shown using Eq. (4) that

$$T_t = T_\tau + \frac{r(\tau_2) - r(\tau_1)}{c_0} \tag{11}$$

Thus, on approach $r(\tau_2) < r(\tau_1)$, so that $T_t < T_\tau$. For a receding aircraft $r(\tau_2) > r(\tau_1)$, which implies that $T_t > T_\tau$. These are the well-known signal compression and expansion effects seen by a ground observer that result in spectral shifts in the frequency domain.

For small smear angles, Eq. (8) will reduce to

$$P_1(\boldsymbol{x}, f) = r_m \frac{e^{-j2\pi fr/c_0}}{r(1 - M\cos\theta)^{n-1}} P_m[\theta, \phi, f(1 - M\cos\theta)] \tag{12}$$

where

$$P_m(\theta, \phi, f) = \int_{\tau_1}^{\tau_2} p_m(\theta, \phi, \tau)e^{-j2\pi f\tau}\,d\tau \tag{13}$$

Using Eqs. (12) and (13), an equation can be derived relating the measured and source narrow-band spectra:

$$\overline{p_1^2(f)} = \frac{\overline{p_m^2[f(1 - M\cos\theta)]}}{(r/r_m)^2(1 - M\cos\theta)^{2n}} \tag{14}$$

Here, it is assumed that r, M, and θ are constant over the time window used in the Fourier transform. Equation (14) explicitly shows the Doppler frequency shift relation, which can be expressed as

$$f_R = \frac{f_S}{1 - M\cos\theta} \tag{15}$$

Converting Eq. (14) to sound-pressure levels produces

$$L(f) = L_m(f) - 20\log(r/r_m) - 20n\log(1 - M\cos\theta) \tag{16}$$

This equation is valid for either bin levels or overall levels. For $n = 2$, a significant increase in sound pressure level (SPL) in the forward arc of the source as the speed increases is predicted by Eq. (16). In particular, directly in front of a source moving at $M = 0.9$, Eq. (16) shows a 40 dB increase in SPL due to motion.

Atmospheric absorption is ignored in the previous discussion. Since absorption of sound increases with frequency and in the forward arc ($-90 < \theta < 90$ deg) the observer spectrum is shifted to higher frequencies, Doppler amplification will be reduced.

Signal De-Dopplerization Procedure

Equation (5) shows that nonstationarity in the measured pressure-time history by a ground observer represented by $p_1(\boldsymbol{x}, t)$ is due not only to any intrinsic nonstationarity in p_m,

but also due to the time-dependent nature of the denominator terms. The basic idea in the de-Dopplerization procedure is to generate a quasistationary signal by rewriting Eq. (5) as

$$p_m(\theta, \phi, \tau) = [r(\tau)/r_m][1 - \boldsymbol{M}(\tau)\cdot\boldsymbol{n}_r(\tau)]^n p_1(\boldsymbol{x}, \tau) \quad (17)$$

where the measured signal p_1 is now expressed as a function of τ. Radar tracking data provided $\boldsymbol{r}(\tau)$ and $\boldsymbol{M}(\tau)$. Equation (4) allows p_1 to be expressed as a function of τ. Ideally, this will render a quasistationary signal where the main cause for spectral variability during flyover measurements will be due to source directivity.

Taking the Fourier transform of Eq. (17) with respect to τ will result in the source spectrum with corrections for amplitude and frequency:

$$P_m(\theta, \phi, f) = \int_{\tau_1}^{\tau_2} \left[\frac{r(\tau)}{r_m}\right][1 - \boldsymbol{M}(\tau)\cdot\boldsymbol{n}_r(\tau)]^n p_1(\boldsymbol{x}, \tau) e^{-j2\pi f\tau}\, d\tau \quad (18)$$

The limitations of this method are 1) the assumption of a quasistationary source in the source reference frame, 2) no atmospheric absorption, 3) assumption of a uniform atmosphere, and 4) ignores ground impedance although the influence of the ground can be minimized by mounting the microphones on ground boards.

The first step in implementing the signal restoration procedure is to designate an initial emission angle and compute x_s, the position of the aircraft along the microphone array axis (see Fig. 1), using

$$x_s = h \cot \theta \quad (19)$$

With this value for x_s, the aircraft position history is searched until x_s is nested, then linear interpolation is used to determine τ, y_s, and z_s. This gives $\boldsymbol{x}_s(\tau)$, which then allows $\boldsymbol{r}(\tau)$ to be computed using Eq. (3), where $\boldsymbol{x}$ represents the microphone location. Next, θ is updated by way of

$$\theta = \cos^{-1}(\boldsymbol{U}\cdot\boldsymbol{r}) \quad (20)$$

The acoustic data $p_1(\boldsymbol{x}, \tau)$ is in a digital format consisting of equally spaced samples. Equation (4) is employed to compute t that corresponds to τ. In general, the reception time spacing is going to vary for evenly spaced emission times. Linear interpolation is performed on the pressure time history to estimate $p_1(\boldsymbol{x}, \tau)$. Incrementing τ by the designated sample rate $\Delta\tau$ generates an equally spaced pressure time history, which is the required form for the fast Fourier transform (FFT) algorithm. As noted previously, the FFT time windows obey $T_t < T_\tau$ on approach and $T_t > T_\tau$ for a receding aircraft. For comparison, uncorrected spectra are constructed and it will be preferable to have equal time windows to obtain the same frequency resolution. Thus, in the displayed measured spectra, the observer time window is extended on aircraft approach and truncated on aircraft recession.

Analysis of Signals with Tones

To demonstrate the de-Dopplerization technique, an aircraft signal containing distinct tones is first considered. The data were acquired from an XV-15 tilt-rotor flyover test[7] in the airplane mode ($M_A = 0.33$, $h = 250$ ft). A linear microphone array composed of four microphones was employed for the far-field acoustic measurements. Figure 2 contains the measured time history for microphone 1 where $\theta_1 = 10.95$ deg. Figure 3 shows the corresponding de-Dopplerized time history using Eqs. (4) and (17) with $n = 2$. Here, $r_m = 62.5$ ft, which is five times the propeller radius of the XV-15. Also, the plot in Fig. 3 was constructed using equally spaced samples determined by the previously described interpolation scheme.

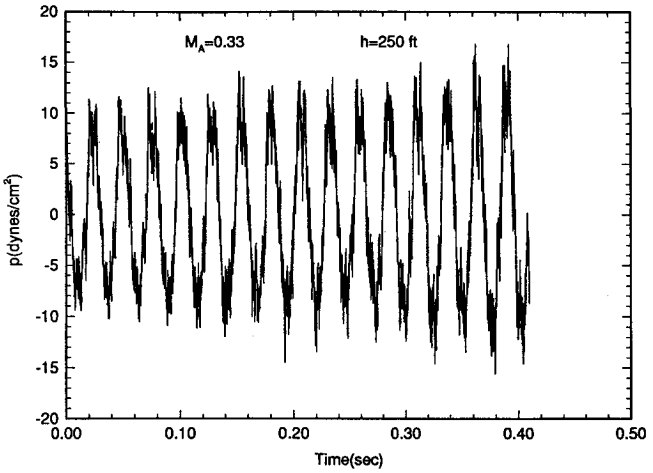

Fig. 2 Measured time history of XV-15 flyover noise, $\theta_1 = 10.95$ deg.

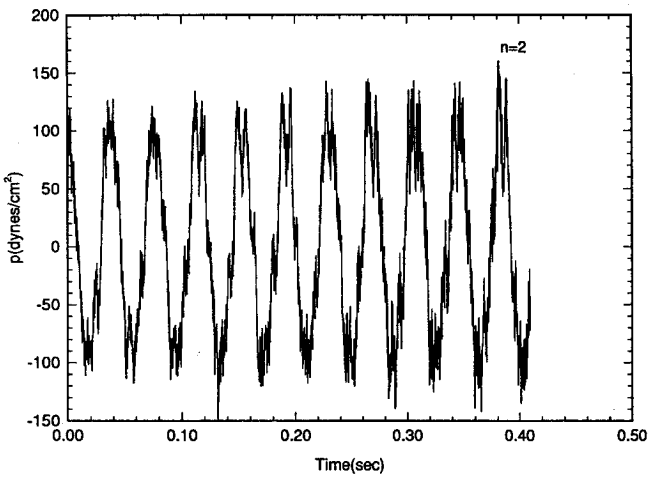

Fig. 3 XV-15 de-Dopplerized time history based on Eqs. (4) and (17), $\theta_1 = 10.95$ deg.

This is the time history that is the input to the FFT algorithm that produces the de-Dopplerized spectrum. Signal compression in the measured time history is clearly seen by comparing Figs. 2 and 3. For this test flight, the propellers were operated at 517 rpm, which yields a blade passage frequency of 25.85 Hz. Notice that an effective period of 0.039 s can be ascribed to the signal in Fig. 3 that yields a fundamental of 25.64 Hz. Remember that the de-Dopplerized signals are computed via Eqs. (4) and (17). Therefore, the signals are corrected for spherical spreading and Doppler amplitude in addition to time distortion (frequency shifts). With these corrections, variability in the de-Dopplerized spectra is due primarily to source directivity. Also, the correction for spherical spreading will result in higher levels for the de-Dopplerized spectra. No correction for spherical spreading was made on the measured data.

Both measured and de-Dopplerized spectra are depicted in Figs. 4–6 for approach, overhead, and recession regimes, respectively. The frequency bandwidth for these spectra is 1.53 Hz. Shown in Fig. 4 is the spectra for $\theta_1 = 10.95$ deg, and clearly seen in the de-Dopplerized spectrum is the fundamental near 26 Hz and the first four overtones near 52, 78, 104, and 130 Hz. This demonstrates that frequency shifts are correctly predicted by the technique.

In Fig. 5, the spectra for $\theta_1 = 53.71$ deg is shown. These spectra contain a large smear angle of $\Delta\theta = 55.73$ deg, which includes the overhead position. Therefore, the first portion of the time history consists of an approach phase with a smear

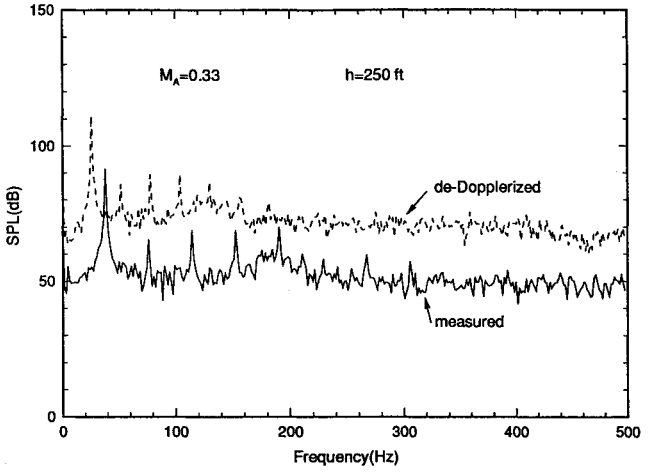

Fig. 4 XV-15 spectra, $\theta_1 = 10.95$ deg, $\Delta\theta = 4.3$ deg.

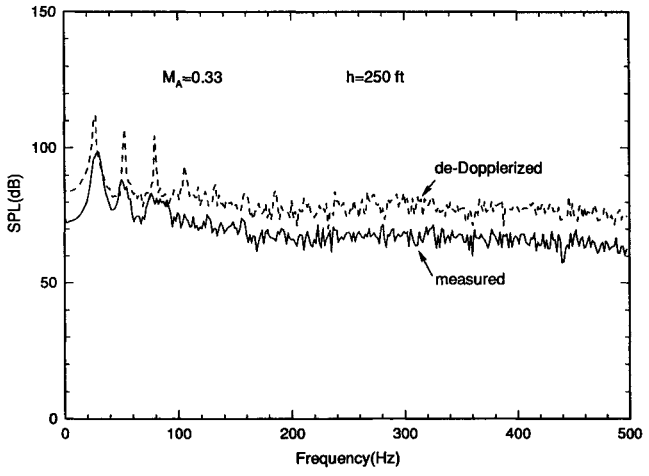

Fig. 5 XV-15 spectra, $\theta_1 = 53.71$ deg, $\Delta\theta = 55.73$ deg.

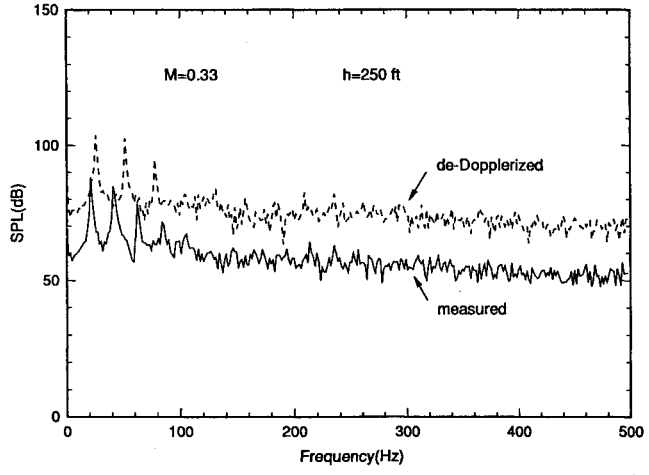

Fig. 6 XV-15 spectra, $\theta_1 = 129.2$ deg, $\Delta\theta = 19.41$ deg.

angle of 36.29 deg and the latter portion consists of a recession phase with a smear angle of 19.44 deg, so that initially there is an upward shift in the spectrum followed by a downward shift. The fourth and fifth harmonics disappear in the measured spectrum due to smearing. Readily evident is the increase in smearing with increasing frequency as typified by the severe spectral smearing in the third harmonic.

Figure 6 illustrates spectra corresponding to $\theta_1 = 129.2$ deg. There appears to be a tone at the third overtone line, 104 Hz, in the de-Dopplerized spectrum. This would shift to 83 Hz in the measured spectrum and a tone does occur in the vicinity of this value. A tone is discernible at the fifth harmonic, 130 Hz, in the de-Dopplerized spectrum. This would be downshifted to 104 Hz in the measured spectrum, but it appears that a distorted tone occurs near this frequency in the measured spectrum. Tones are located at the seventh and eighth overtone lines, 208 and 234 Hz, in the de-Dopplerized spectrum, but are not apparent in the measured spectrum.

Analysis of Jet Noise Broadband Signal

The signal restoration procedure is now applied to data characterizing jet noise. Although jet noise is generally characterized as being broadband in nature, it can exhibit screech tones and spectral peaks due to the presence of shocks in the jet.[6,8] Correcting for motion could sharpen any tones or spectral peaks contained in the recorded signal. Due to the higher flight velocities of jet-powered aircraft, de-Dopplerized signals could also be of value in determining the Doppler amplitude factor, i.e., n in Eq. (5). Spectra constructed from data collected during an F-18 flyover are shown in Figs. 7–9, where $M_A = 0.8$ and $h = 1500$ ft. For the de-Dopplerized spectra, n was given a value of 2 and $r_m = 1$ ft. In Fig. 7, the spectra correspond to $\theta_1 = 16.19$ deg with $\Delta\theta = 0.89$ deg. Spectral peaks characteristic of broadband shock-associated noise are evident in the measured spectrum. These peaks are centered at 600, 1200, and 1800 Hz. The structure in the vicinity of 3 kHz is extraneous noise generated by the data

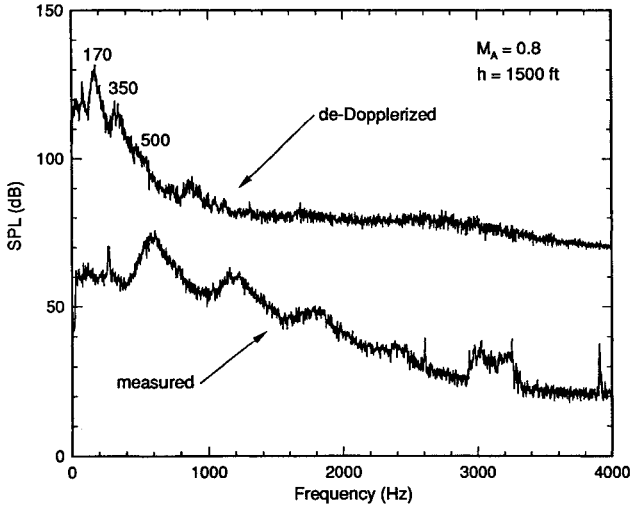

Fig. 7 F-18 spectra, $\theta_1 = 16.19$ deg, $\Delta\theta = 0.89$ deg.

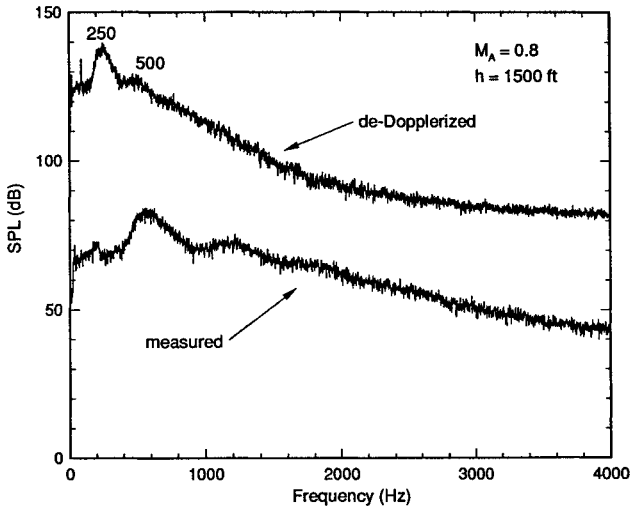

Fig. 8 F-18 spectra, $\theta_1 = 36.51$ deg, $\Delta\theta = 6.4$ deg.

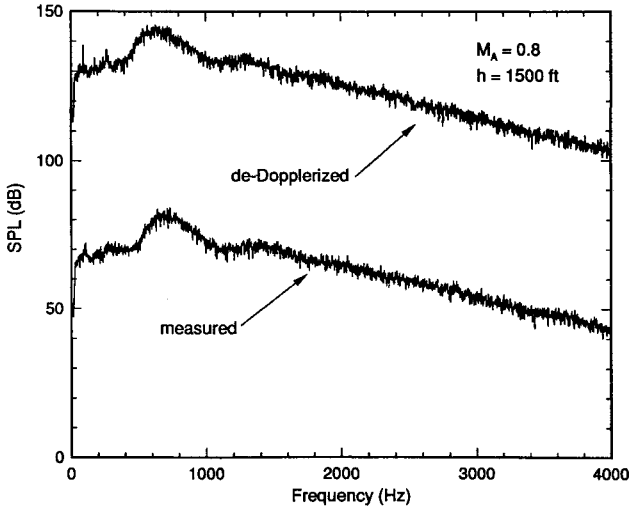

Fig. 9 F-18 spectra, $\theta_1 = 75.84$ deg, $\Delta\theta = 15.5$ deg.

acquisition system. In the de-Dopplerized spectrum these peaks shift to 170, 350, and 500 Hz, respectively. The peak near 850 Hz results from the noise structure at 3 kHz in the measured data. Note the narrowing of the spectral peaks due to the de-Dopplerization procedure.

Figure 8 shows the spectra for $\theta_1 = 36.51$ deg with $\Delta\theta = 6.4$ deg. A dominant peak occurs at 560 Hz and a secondary peak at 1215 Hz in the measured spectrum. Minor peaks also appear at 40 and 200 Hz, which produce distinct tones at 15 and 80 Hz, respectively, in the de-Dopplerized spectrum. The peaks at 560 and 1215 Hz shift to 250 and 500 Hz, respectively, in the de-Dopplerized spectrum and are narrower compared to the measured spectrum. As would be expected, the frequency shifts are not as great as those exhibited in Fig. 7, mainly because of the larger emission angle.

The case for $\theta_1 = 75.84$ deg with $\Delta\theta = 15.5$ deg is depicted in Fig. 9 so that this includes the overhead position of the aircraft. Although Doppler shifts should be slight since the aircraft is in the overhead region, spectral smearing could be significant because of the rather large smear angle associated with the spectra. In the measured spectrum a tonal peak is detectable at 100 Hz and there is a slight rise in the spectrum in the vicinity of 280 Hz. The de-Dopplerized spectrum shows sharp tones occurring at 80 and 250 Hz. For the measured spectrum, the maximum peak is centered at 710 Hz and a secondary peak exists at 1390 Hz. These shift to 625 and 1300 Hz, respectively, with only a slight change in spectral shape.

By comparing the de-Dopplerized spectra in Figs. 7–9 and other spectra not presented, the characteristic features of broadband shock-associated noise are more readily evident. These spectra confirm previous observations that the peak frequency increases as θ increases[9] and that the spectral width of the dominant peak narrows as θ decreases.[10]

To assess the effect of correcting for the time dependence of spherical spreading and Doppler amplitude, $p_1(x, \tau)$ [see Eq. (17)], was constructed to be the input signal into the FFT algorithm. This is just the measured signal corrected only for time distortion by way of Eq. (4). Figure 10 compares the spectrum generated by this signal with the de-Dopplerized spectrum of Fig. 7 for the case of a small smear angle, $\Delta\theta = 0.89$ deg. The spectra are identical in frequency content. The conclusion based on Fig. 10 and other data not presented is that as far as the de-Dopplerized spectral shape is concerned, it appears to be solely determined by correcting for time distortion in the signal. It is unaffected by corrections for spherical spreading and Doppler amplitude.

It is difficult to validate Eq. (17) for amplitude effects from flyover test data. Probably, it would be more definitive and yield better results to design a wind-tunnel experimental procedure in order to determine flight effects. Having a carefully controlled environment and a known source structure would enhance the confidence of any attempt to determine source influence on the observed acoustic signals. These results that would be valid in the aircraft reference frame could then be converted to a ground-based reference frame.

Table 1 Overall sound pressure levels

θ_1, deg	$\Delta\theta$, deg	$n = 0$, dB	$n = 1$, dB	$n = 2$, dB
16.19	0.89	161.3	149.8	138.4
36.15	6.40	165.4	157.7	150.1
75.84	15.50	162.4	161.6	160.6
90.00	15.62	160.2	161.0	161.9
104.26	13.77	162.0	164.4	166.8
133.48	7.30	167.8	171.7	175.7

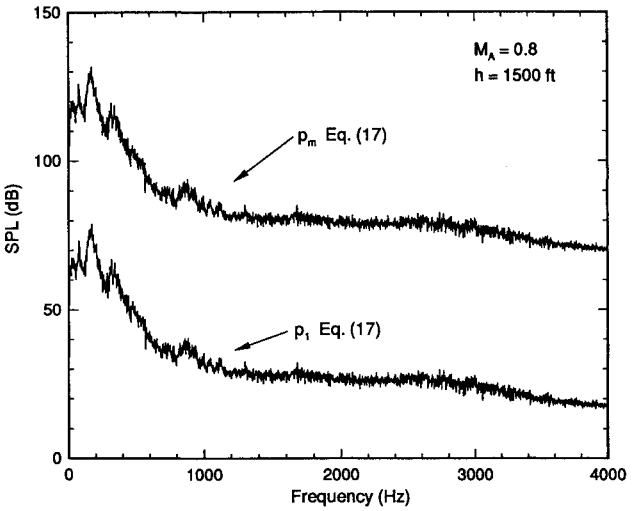

Fig. 10 Time correction comparison, $\theta_1 = 16.19$ deg, $\Delta\theta = 0.89$ deg.

Values for n are determined by the nonhomogeneous term on the right-hand side (RHS) of Eq. (1). The time and space derivatives result in $n = 2$. If these operators are absent then $n = 1$.[5] With these comments in mind, SPLs were computed at the source for differing values of n. As stated previously, the de-Dopplerized amplitudes will be higher due to the correction for spherical spreading alone. The correction for Doppler amplitude decreases the source amplitude in the forward arc, but increases it to the rear. In this study, both corrections are made to the measured data in order to remove nonstationarity from the signal.

Considering the above flyover again, overall-sound pressure levels at the source were calculated for six emission angles. Level values were determined for the time history generated by Eq. (17), p_m, for $n = 0$, 1, and 2. The results are tabulated in Table 1 where 6 dB has been subtracted from all of the levels to account for ground effects. For $n = 0$, the source directivity pattern is essentially uniform showing little variation between forward and rearward arcs. Significant differences appear between fore and aft directions for $n = 1$ and are still greater for $n = 2$. The levels differ the least at $\theta_1 = 75.84$ and 90 deg, which is due to the Doppler amplitude having little influence in the overhead region. In general, overall-sound pressure level (OASPL) increases towards the jet axis where the highest value occurs at $\theta_1 = 133.48$ deg for $n = 2$. Therefore, this indicates that the dominant noise component in these measurements is due to turbulent mixing noise since little broadband shock noise is radiated at this angle.

Summary

A de-Dopplerization scheme was devised and applied to both a tonal noise source XV-15, and a broadband noise source

F-18. The de-Dopplerized time history was constructed by using linear interpolation in the measured time history. This was made possible by knowing the position history of the aircraft provided by radar and/or laser tracking. It was advantageous to consider the tonal source since the blade passage frequency of the rotors provided distinct reference tones. Tonal peaks were accurately constructed at the correct frequencies in the de-Dopplerized spectra determined from the XV-15 data.

The higher flight speed of the F-18 aids in assessing the influence of spherical spreading and Doppler amplitude on the received signal. Taking F-18 measured data acquired during a flyover test that exhibited the presence of broadband shock noise allowed the de-Dopplerization procedure to be applied to a signal containing spectral peaks. These spectral peaks and tonal features appeared sharpened in the de-Dopplerized spectra. Also, this analysis confirmed what has been noted in prediction models and static tests, namely, that the peak frequency increases and the peaks broaden toward the jet axis. Using this data showed that correcting for spherical spreading and Doppler amplitude had no effect on spectral shape. Overall SPLs were computed from the corrected signals for three values of the Doppler exponent, $n = 0$, 1, and 2. Variation in the directivity pattern increased with n. Since the highest source levels occur as the jet axis is approached, this suggests that the dominant noise mechanism in jet noise is turbulent mixing.

Acknowledgment

This study was supported by NASA Langley Research Center Contract NAS1-9000.

References

[1]Verhas, H. P., "A Restoration Procedure for (Nonstationary) Signals from Moving Sources," *Journal of Sound and Vibration*, Vol. 89, No. 4, 1983, pp. 487–497.

[2]Howell, G. P., Bradley, A. J., McCormick, M. A., and Brown, J. D., "De-Dopplerization and Acoustic Imaging of Aircraft Flyover Noise Measurements," *Journal of Sound and Vibration*, Vol. 105, No. 1, 1986, pp. 151–167.

[3]Kelly, J. J., "Signal Processing of Aircraft Flyover Noise," NASA CR 187546, May 1991.

[4]John, F., *Partial Differential Equations*, Springer–Verlag, New York, 1975.

[5]Dowling, A. P., and Ffowcs Williams, J. E., *Sound and Sources of Sound*, Ellis Horwood, Chichester, England, UK, 1983, Chap. 9.

[6]Tam, C. K. W., "Broadband Shock Associated Noise of Supersonic Jets Measured by a Ground Observer," AIAA Paper 92-0502, Jan. 1992.

[7]Golub, R. A., Becker, L. E., Rutledge, C. K., Smith, R. A., and Conner, D. A., "Some Far-Field Acoustics Characteristics of the XV-15 Tilt-Rotor Aircraft," AIAA Paper 90-3971, Oct. 1990.

[8]Norum, T. D., and Seiner, J. M., "Measurements of Mean Static Pressure and Far Field Acoustics of Shock Containing Supersonic Jets," NASA TM 84521, Sept. 1982.

[9]Harper-Bourne, M., and Fisher, M. J., "The Noise from Shock Waves in Supersonic Jets," *Noise Mechanisms*, AGARD-CP-131, March 1974, pp. 11.1–11.13.

[10]Tam, C. K. W., Seiner, J. M., and Yu, J. C., "Proposed Relationship Between Broadband Shock Associated Noise and Screech Tones," *Journal of Sound and Vibration*, Vol. 110, No. 2, 1986, pp. 309–321.